Lawrence Berkeley Laboratory
UNIVERSITY OF CALIFORNIA

Accelerator & Fusion Research Division

Submitted to Physical Review A

IONIZATION OF RARE-GAS TARGETS BY COLLISIONS OF FAST HIGHLY CHARGED PROJECTILES

A.S. Schlachter, K.H. Berkner, W.G. Graham, R.V. Pyle, P.J. Schneider, K.R. Stalder, J.W. Stearns, J.A. Tanis, and R.E. Olson

October 1980

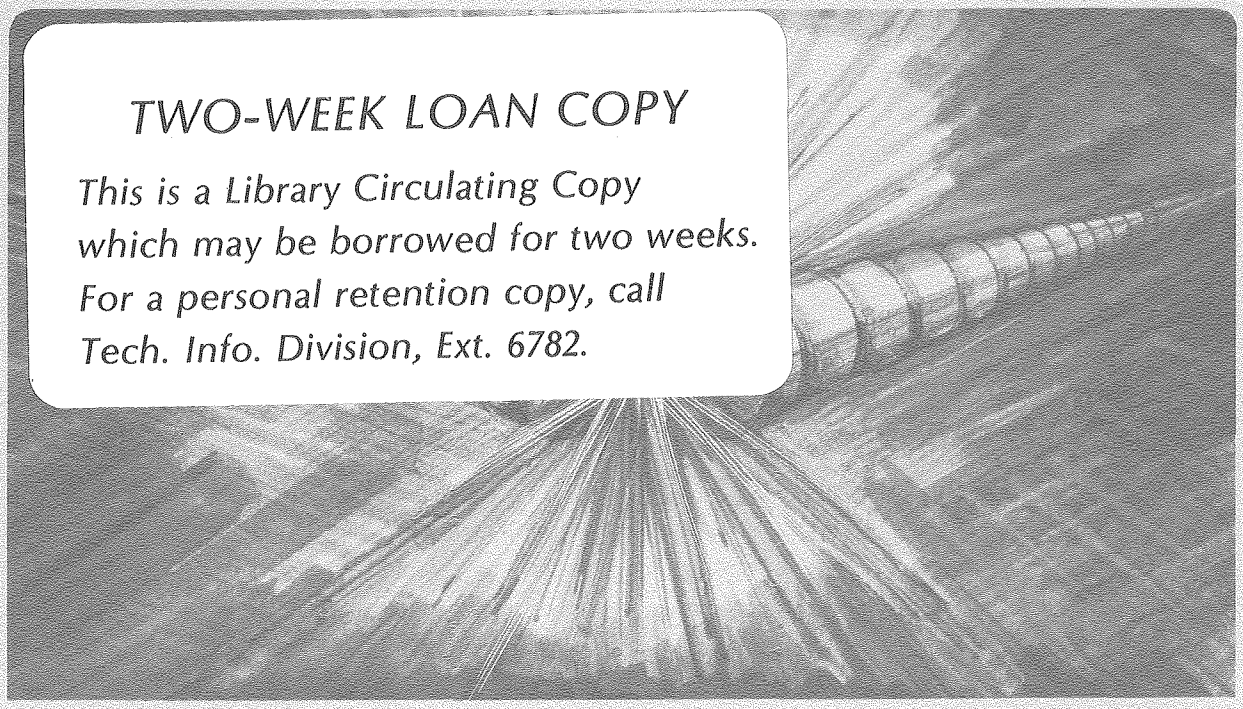

Prepared for the U.S. Department of Energy under Contract W-7405-ENG-48

DISCLAIMER

Submitted to Physical Review A LBL-10944

Ionization of Rare-Gas Targets by Collisions of Fast Highly Charged Projectiles

A. S. Schlachter, K. H. Berkner, W. G. Graham*
R. V. Pyle, P. J. Schneider+, K. R. Stalder
J. W. Stearns and J. A. Tanis‡

Lawrence Berkeley Laboratory
University of California
Berkeley, California 94720

R. E. Olson

Molecular Physics Laboratory
SRI International
Menlo Park, California 94025

ABSTRACT

We have determined the net ionization cross section for total slow-ion or slow-electron charge production in rare-gas targets by passage of a fast projectile both experimentally and theoretically. We have experimentally studied ionization in these targets by C, Fe, Nb, and Pb projectiles with energies ranging from 310 keV/amu to 4.8 MeV/amu and for charge states in the range of +4 to +54. Theoretical calculations employing the classical-trajectory Monte-Carlo method are used to calculate ionization cross sections in the rare gases for projectiles at collision energies of 1 MeV/amu to 5 MeV/amu with charge states +5 to +80. Experiment and theory generally agree within a factor of 2 over this wide range of conditions. For a given rare-gas target, the cross sections for net ionization reduce to a common curve when plotted as cross section divided by charge state versus energy per nucleon divided by charge state.

PACS number: 34.70.+e and 34.50 Hc.

10/22/80

I. INTRODUCTION

Ionization of atoms by fast, highly charged projectiles has been studied mainly from the viewpoint of inner-shell[1] processes in which cross sections are determined by observing x rays or Auger electrons. Previous experiments in which slow-ion or slow-electron charge is collected in the target to measure net ionization have usually used protons or other light projectiles.[2] We have previously reported[3,4] cross sections for ionization of H_2 by fast iron ions in charge states 3–22 for energies ranging from 103 keV/amu to 3.4 MeV/amu. In this paper we present a series of measurements and theoretical calculations for ionization of the rare gases by a wide variety of highly charged projectiles.

The charge-state spectrum of recoil ions produced in a rare-gas target by passage of a fast high-charge-state projectile beam has recently been measured by Cocke,[5] who used a high-efficiency time-of-flight spectrometer to measure the charge-state spectrum of recoil ions produced by single collisions of 0.67–1.2 MeV/amu chlorine ions with rare-gas targets. Cross sections σ_j for production of target recoil ions j-times ionized were obtained. Haugen et al.[6] have recently begun similar studies with gold projectiles. Beyer et al.[7] have used slow recoil ions in electron-capture cross-section measurements.

The cross sections reported in the present work were measured by the condenser-plate method, in which slow ions and electrons are collected in the target. If σ_j is the cross section for producing a target ion j-times ionized, then the net ionization cross section, σ_+, is

$$\sigma_+ = \sum j \, \sigma_j \, . \qquad (1)$$

This is the total cross section for producing positive ion charge in the target.

We have also previously reported[3,8] ionization cross sections calculated by the classical-trajectory Monte Carlo method (CTMC) for collisions of highly charged ions in charge states +1 to +50 with atomic hydrogen at energies from 50 keV/amu to 5 MeV/amu. The CTMC method has also been applied to He targets[9] for 100-500 keV/amu projectiles in charge states up to +8. Agreement with experiment is good for both ionization and electron capture, which are calculated simultaneously in the CTMC method. Advantages of the CTMC method are that it is non-perturbative and preserves the unitarity of the S-matrix.

The three-body, three-dimensional CTMC method can also be applied to multi-electron targets.[10] Transition probabilities are obtained as an intermediate step in the cross-section evaluations. By using an ionization energy and an effective charge that characterize an electron shell of a multiple-electron target atom, multiple-electron ionization cross sections may be calculated using the independent-electron model developed by Hansteen and Mosebekk[11] and by McGuire and Weaver.[12] We have previously performed such calculations[10] for 1 MeV/amu projectiles in charge states +2 to +20 colliding with He, Ne, and Ar targets; good agreement was found with our measured net-ionization cross sections.

In 1978 we reported[13] a scaling rule for the energy and charge-state dependence of electron loss from a hydrogen atom in collision with a fast, highly charged projectile ion. This scaling rule

was based on theoretical CTMC calculations. The experimental confirmation was based on measurements with iron projectiles in a molecular hydrogen target, where, at all but the lowest energies, the H_2 target was treated as two H atoms for comparison with the calculations. We have also reported[9] a scaling rule of similar form for low-energy, low-charge-state projectiles on a helium target, where multiple ionization was not considered.

In this article we present measurements[14] of net ionization cross sections for C, Fe, Nb, and Pb projectiles in charge states +4 to +54 and for energies from 310 keV/amu to 4.8 MeV/amu colliding with He, Ne, Ar, and Xe targets, and CTMC ionization calculations for ions in charge states +5 to +80 with energies from 1-5 MeV/amu in He, Ne, Kr, Ar, and Xe. Experimental results are compared with the calculations, which generally agree to better than a factor of 2. We also obtained charge-state and energy scaling rules for net ionization valid for a wide variety of projectile energies and charge states for each rare-gas target.

II. THEORETICAL METHOD

The theoretical calculations use the CTMC method to determine the transition probabilities within a one-electron formalism and then extend these transition probabilities to represent a multi-electron target by use of the independent electron model.[11,12] We employ a three-body, three dimensional CTMC method[8] that includes all forces between the incident ion, active electron and target nucleus. The independent electron model requires for validity that the collision be sudden, with the collision period sufficiently brief that the electrons cannot rearrange themselves during the collision. Hence, this model is only valid for collision velocities at least several times greater than the orbital velocities of the electrons being detached. The model ignores correlation effects between the electrons in a given shell.

In the independent-electron model, the multiple ionization transition probabilities $P_n(b)$ for removing n electrons from a shell containing N electrons for a collision at an impact parameter b are given by:

$$P_n(b) = \binom{N}{n} P_s(b)^n \, [1-P_s(b)]^{N-n} \qquad (2)$$

where $\binom{N}{n}$ is the binomial coefficient and $P_s(b)$ is the transition probability calculated in a one-electron model. Equation (2) can be easily extended to allow for electron detachment out of several shells of a given atom. In fact, we have included several electron shells in our calculations on Ar, Kr, and Xe targets. We did not account for

cascade effects after the collision, which would tend to increase the multiple ionization. Hence, our cross-section calculations for production of high states of ionization can only be considered qualitative. Fortunately, the inner-shell cross sections are quite small when compared to the outer-shell values.

The application of Eq. (2) requires one-electron transition probabilities $P_s(b)$ as input parameters. In order to obtain these, the CTMC method was employed. The calculational procedure for the CTMC method has previously been described in detail[8] and is based on solving Hamilton's equations-of-motion for a three-body system (12 coupled first-order differential equations). The coupled equations must be solved many times within the framework of the Monte-Carlo method to obtain an accurate description of the electron distribution about the target nucleus and to span the impact parameters required to describe the collision. In the present calculations, 2,000 to 10,000 trajectories for each charge state, electron shell and collision energy were adequate to determine transition probabilities of sufficient accuracy to employ the independent electron model.

Since the CTMC method is only directly applicable to hydrogenic target atoms, it is necessary to extend the representation of the target electron so that it profiles the electron shell under consideration. Such an extension requires that we determine an effective charge Z_{eff} of the target nucleus as seen by the active electron. We require that two conditions be met. The first is that the binding energy U of an electron in a shell be correct so that threshold energy behavior is accurately portrayed. The second condition is that the radial size of the simulated electron cloud must be reproduced so that the dimensions of the target atom are close to reality.

Within the confines of the classical hydrogenic model employed here, the above two conditions require that the expectation value of the active electron be given by

$$\langle R \rangle = Z_{eff}/(-2U) \qquad (3)$$

where U is the electron binding energy in atomic units. In our calculations, we used the <R> and U Hartree-Fock values of Fischer[15] to determine Z_{eff}. The values of Z_{eff} used were 1.69 for He, 2.12 for the L-shell of Ne, 7.89 for the L-shell and 2.45 for the M-shell of Ar, 6.68 for the M-shell and 2.55 for the N-shell of Kr, and 18.06, 7.29 and 2.61 for the M, N, O-shells of Xe. The M-shell of Xe was only included in the 5-MeV/amu calculations for incident ion charge states $q \geq 20$.

In the calculations, we have assumed the projectile is fully stripped. Thus, the theoretical results will tend to underestimate the cross sections for partially stripped ions in low states of ionization for a given charge state due to (1) the neglect of interactions of projectile electrons with target electrons, and (2) the fact that the target atom will see a higher effective charge for small impact-parameter collisions which penetrate the electron shells of the projectile.

III. EXPERIMENTAL METHOD

A. General description

We used the method of slow-ion and slow-electron collection to measure the net ionization cross section for a projectile A^{+q} in charge-state q colliding with a target atom. Net ionization means we collected all the ion or electron charge produced in the target along a well-defined path length. We have described our methods in detail in Ref. 4 and shall give only a brief discussion here.

A schematic view of the apparatus is shown in Fig. 1. A fast heavy ion beam from the Berkeley SuperHILAC was post-stripped in a carbon foil, giving a distribution of high charge states, one of which was selected by the charge-selection magnet. The charge state and energy of the projectiles were determined by deflecting the beam onto a fixed-position solid-state detector located behind a slit. The spectrometer magnet was previously calibrated by a wire-orbit technique. Energy loss in the foil was estimated from the calculated stopping power[16], which we confirmed with our spectrometer magnet. Uncertainty in the energy was 1-3%.

The incident beam was collimated by two circular apertures, C_1 and C_2, shown in Fig. 1, whose diameters were 3.2 mm and 2.5 mm. This limited the beam to a diameter smaller than those of apertures C_3 - C_5 (3.3 mm, 3.3 mm, and 3.8 mm diameter, respectively), so that no beam was lost in the target nor at the Faraday cup detector. Collimators C_2 and C_5 isolated the differentially pumped section of the target from the beamline.

Slow ions and electrons produced by ionization or charge transfer were swept from a well-defined length of the target chamber by a variable weak electric field applied between a pair of 3-cm-long plates spaced 1 cm apart, and were collected on one of these plates. Guard plates were used to provide a uniform transverse electric field. We increased the voltage applied to the plates until the collected current was insensitive to further increases.

The spectrometer magnet located after the target deflected the primary beam into the center cup of a double Faraday cup assembly, while those ions that captured or lost electrons were collected in the outer cup of the assembly. The ratio of the charge-transferred beam to the primary beam was less than 10% in all cases. Secondary-electron emission was suppressed in both Faraday cups by the magnetic field of the spectrometer magnet.

Net ionization cross sections were determined by simultaneously measuring the slow ion or electron current to one of the collector plates in the target and the fast ion current collected on the Faraday cup downbeam from the target. The electrometer signals were integrated over a period of several electrometer time constants; a typical integration time was 30 seconds. Measurements were made for at least ten different pressures. The data were corrected for charge transfer in the target; this correction was usually less than 1%. The least-squares fit of the ratio of the integrated collector current to integrated projectile-ion particle current, as a function of target thickness, gave the ionization cross section.

For lead projectiles a different procedure was used to measure ionization cross sections. Because the incident beam intensity was only of the order of 10^3 lead ions/sec, which, at charge +50, is less than 1×10^{-14} amps, we had to count the lead ions with a solid-state detector (described in Ref. 4). The ionization cross sections were so large, however, that we were able to obtain sufficient slow ion or electron current on the collection plate to measure the current with an electrometer. The ionization cross section in this case was determined from the ratio of integrated collector current to integrated incident particles in the projectile beam, expressed as a particle current.

B. Secondary-electron emission from collector plate

Secondary electrons from the collector plate, swept by the transverse electric field in the target, increase the apparent current at each electrode; if not accounted for, this secondary emission would cause the ionization cross section to appear erroneously large. To check the magnitude of this effect we performed a separate experiment on a 150-keV accelerator, which used the same target cell as was used at the SuperHILAC, since space limitations precluded the use of magnetic suppression during the cross-section measurements. By means of two large-diameter coils coaxial to the beam and located symmetrically ahead of and behind the target, we were able to magnetically suppress secondary-electron emission from the collector plate. A beam of 120-150 keV D^+ ions was passed through the target, and the resulting beam-normalized slow-ion collector current was monitored while the transverse electric field and the magnetic field were varied, at various target pressures. Secondary electrons were considered to be suppressed

when a change in the magnetic field produced no change in the collected ion current. It was further verified that the collected current did not change with an increase in electric field, the usual condition for complete ion collection. About 200 gauss at the center of the target was required to suppress secondary electrons under normal conditions of electric field (120 V/cm) and target pressure (10^{-2} Torr).

We found that the decrease in observed collector current with suppression depended on the target gas; we also found a correlation between ionization potential of the gas and secondary emission. For Ar there was no decrease in collected current with suppression within the sensitivity of the measurement (2%). We found a 6% decrease in current when Ne was the target gas, and 8% for He. We made no measurements of electron suppression in Xe; we assume the same value as in Ar, since the ionization potentials are similar.

The mean charge state of recoil ions was higher in the experiments with heavy-ion projectiles than in the electron-suppression tests. We know of no measurements of secondary-electron-emission coefficients for multiply charged ions impacting on dirty metal surfaces; however, for clean surfaces,[17] a pronounced energy and charge-state dependence for secondary-electron emission has been reported. The insensitivity of our cross-section measurements to the collector bias voltage (recoil-ion energy) suggests that any effect due to multiply charged ions is small. Another indication that this effect is small is the observed linear pressure dependence of the collected ion current. The charge state of a recoil ion is reduced by electron capture, which is large[18,19] for a highly charged ion in its parent gas.

We applied correction factors determined in the electron-suppression tests to the measured cross sections: we reduced the ionization cross sections in He by the factor 0.92, in Ne by 0.94, and made no correction to cross sections in Ar and Xe. We estimate the average uncertainty introduced by these corrections to be ±5%. The higher average charge state of the recoil ions in the cross-section measurements could cause the cross sections to be too high by an estimated 10%.

C. Uncertainties

The net-ionization cross sections have the following sources of relative uncertainty: linear least-squares fit to the data which includes zero drift and fluctuations in the electrometers and in the capacitance manometer (typically 5%), corrections for second-order processes (2%), scale-to-scale variations in the electrometer-integrator system (3%), choice of electric field in collection region (5%), and uncertainty in the correction factors for secondary-electron emission from the collector plates (5%). Typical standard relative uncertainty is thus 10%. We estimate the systematic uncertainties to be 4% for the target thickness, 2% for beam loss on collimators, 2% for differences in using slow-electron or slow-ion charge to determine σ_+, and 10% (decrease only) for secondary-electron emission effects. Combining the relative and systematic uncertainties we estimate the typical absolute standard uncertainty in our experimental net-ionization cross sections to be +11% and -15%.

IV. RESULTS AND DISCUSSION

A. Experimental and theoretical results

Experimental results for the net ionization cross sections for various projectiles and targets are given in Figs. 2-5 and in Table I for projectile energies of 310 keV/amu, 1.1 MeV/amu, 3.4 Mev/amu, and 4.7 MeV/amu. Also shown at the higher energies in Figs. 3-5 are ionization cross sections calculated using the CTMC method combined with the independent-electron model. Agreement between experimental and calculated values is generally better than a factor of 2, which is within the combined uncertainty of the measurements and the calculations.

The 310 keV/amu results shown in Fig. 2 can be extrapolated to compare with theoretical predictions of Bottcher.[20] This author calculates a net ionization cross section of 1.1×10^{-16} cm^2 for C^{+4} + He collisions at 250 keV/amu. Extrapolation of our +5 and +6 results would indicate the measured value is approximately a factor of 8 above this theoretical prediction.

Figure 3 shows the experimental results of Cocke[5] for 0.97 MeV/amu Cl^{+q} projectiles in He, Ne, and Ar targets. We calculated $\sum j \sigma_j$ from his σ_j results to obtain a net ionization cross section for comparison with the present results. To compare cross sections at the same energy, we reduced Cocke's cross sections by the ratio 0.97 Mev/amu to 1.1 MeV/amu, since we found that ionization cross sections are approximately inversely dependent on energy at high energies. His experimental results for q = +6 are almost a factor of 2 larger than our experimental or calculated results. We attribute this to the lower state of ionization of the Cl projectiles relative to the fully stripped

C projectile, which allows the target atom to see a much higher effective charge in small-impact-parameter collisions upon penetration of the remaining Cl electron shells. Also, the additional projectile-electron target-electron interactions for a low state of ionization of an ion will increase the net ionization cross sections above those measured here for a highly stripped ion and those calculated for a completely stripped ion. Cocke's results for Cl^{+12} are in excellent agreement with the calculated net ionization cross section and with our measurement for Fe^{+12} in Ar, which supports these conclusions.

B. Energy and Charge-State Scaling

In previous work on single-electron-detachment collisions (electron capture plus ionization), we obtained a scaling rule applicable to highly stripped ions colliding with hydrogen and helium atom targets.[9,13] The cross sections were found to reduce to a single curve when the cross section divided by projectile charge state was plotted versus the collision energy per nucleon divided by the projectile charge state.

At high energies, such a plot closely approaches the Born approximation result, with the cross sections proportional to q^2/E. At low energies, however, the cross sections approach a limit which is linear in charge state and independent of energy; such behavior can be explained using arguments first presented by Bohr and Lindhard[21] which state that the collision radius for electron detachment is determined by the distance at which the force from the active electron's present nucleus and the force from the highly-charged projectile ion are equal.

We would expect a similar relationship to hold for the net ionization cross sections since these cross sections are directly proportional to the total amount of charge that can be removed from a given target atom. We should note that in our calculations of the net ionization cross section, we include both the direct ionization process of the target and the electron-capture process. The latter process is known[22] to affect the high states of ionization of the target and is an important mechanism for electron removal from inner, tightly bound electron shells.

To test this cross-section relationship, we have calculated the multiple ionization cross sections for highly stripped ions in charge states $q = +5$, $+10$, $+20$, $+40$ and $+80$ colliding with the rare gases at energies of 1 MeV/amu, 2 MeV/amu and 5 MeV/amu. The results are shown in Fig. 6 where, indeed, the reduced cross sections for a given target species are found to reduce to one curve. As seen in Fig. 6, the cross sections are proportional to q^2/E at the highest values of E(MeV/amu)/q and are tending to approach a linear dependence on q at the lowest value of E(MeV/amu)/q. This latter behavior is being approached by the highest charge states where the reaction radii are very large, 20 to 35 a_o.

Of interest is the fact that the reduced plot of Fig. 6 is inapplicable to the cross sections calculated for specific states of ionization, σ_j. Such behavior is expected since the Bohr-Lindhard arguments for the lower reduced energy collisions apply only to the total charge removed from a target atom.

As a test of the theoretical cross-section scaling behavior, we show in Fig. 7 a comparison between theoretical and experimental results.

The experimental data give credence to the scaling relationship and are, in general, within a factor of 2 of the theoretical predictions. Although the absolute magnitudes of σ_+ are qualitatively reproduced, there is a difference in the apparent scaling dependence, for large values of E/q, with theory predicting σ_+ proportional to q^2/E while the experimental data tend toward $q^{3/2}/E^{1/2}$. More experimental data will be required to test the theoretical calculations. It should be emphasized that, although the scaling procedure discussed here is the same as we used for electron loss from hydrogen and helium, the present scaling is different in that multiple ionization is included; multiple ionization was neglected in the previous treatment of He, which was limited to lower energies, where the independent electron model is invalid.

C. Individual Ionization Cross Sections

Although the experimental data presented here do not yield any information on the individual cross sections σ_j for production of target recoil ions j-times ionized, the calculations give some insight into these values. Figure 8 shows the results of our calculations for highly stripped ions colliding with Ar at the energies studied. The calculations are most accurate for the prediction of low states of ionization of the target atom. For high states of ionization the calculated cross sections can only be considered qualitative and have uncertainties of at least a factor of 2 because of neglect of cascade effects and the breakdown of the sudden-impact approximation required for the independent electron model.

As illustrated in Fig. 8, high states of ionization of the target are produced with sizable cross sections by the passage of an energetic high-charge-state ion. Notable are the results for producing ten-times-ionized Ar, where cross sections approaching 10^{-15} cm^2 are predicted for projectile ions in charge states $q \gtrsim 40$.

Plots of the transition probabilities as a function of impact parameter, as previously given in Ref. 10, show that a direct collision of the projectile ion with electrons in a shell of the target atom is not required to remove a large fraction of the electrons from that shell. Rather, the strong Coulomb force of the projectile pulls electrons out of the shell at distances 5 to 15 times greater than the radius of the electrons on the target. In illustration of this point, the theoretical calculations show that impact parameters as large as 30-40 a_0 contribute to the ionization process for highly charged ions colliding with the heavier rare gases. Such large-impact-parameter collisions produce target recoil ions that are very slow, since very little energy is transferred to the target compared with interactions requiring impact parameters close to the electron orbital radius. These slow recoil ions can then be employed in subsequent collision experiments to probe a collision velocity regime that is inaccessible by conventional methods.

V. CONCLUDING REMARKS

We have measured net-ionization cross sections for fast highly stripped projectiles ranging from C^{+4} to Pb^{+54} in rare-gas targets. These net ionization cross sections for highly stripped ions are smaller by a factor of 2 than similar previously reported[5] cross sections measured with less highly stripped projectiles in the same charge state at the same velocity. The difference reflects the higher effective charge seen by the target in small-impact-parameter collisions for the case of the less highly stripped projectile. Ionization cross sections for highly stripped projectiles in rare gases were calculated using the CTMC method with the independent-electron model, for energies from 1-5 MeV/amu, charge states +5 to +80, for He, Ne, Ar, Kr, and Xe targets. Calculations and measurements of net ionization cross sections generally agree within a factor of 2. Calculations of cross sections σ_j for production of j-times-ionized target recoil ions are in qualitative agreement with recent measurements of Cocke.[5] There is better agreement for lower states of ionization of the target atom than for higher states, due to neglect of cascade effects and breakdown of the sudden-impact approximation implicit in the calculations. Ionization cross sections are found to be very large. As an example, the cross section for producing Xe recoil ions ten-times ionized exceeds 10^{-16} cm^2 for projectiles with charge state $\geq$ +40.

Calculated net ionization cross sections can be scaled to a reduced curve for each target species using as reduction parameters the energy per nucleon divided by projectile charge state and the cross section divided by charge state. These reduced curves can be used to predict net ionization cross sections for projectiles with energies from 1-5 MeV/amu, charge states +5 to +80, for any rare-gas target. Experimental results are roughly consistent with this scaling; however, the

experimental cross sections tend to decrease less rapidly with increasing E/q than is predicted theoretically.

ACKNOWLEDGMENTS

This work was supported by the Fusion Energy Division of the U. S. Department of Energy under contracts W-7405-ENG-48 and DEAT03-76ET53025.

References

* Present address: Physics Department, New University of Ulster, Coleraine, Northern Ireland.

+ Present address: PWW Abteilung, Max-Planck-Institut für Plasmaphysik, 8046 Garching bei Munchen, West Germany.

‡ Present address: Department of Physics, Western Michigan University Kalamazoo, MI 49008.

1. P. Richard, in Electronic and Atomic Collisions, Proceedings of the XIth International Conference on the Physics of Electronic and Atomic Collisions: Invited Papers and Progress Reports, edited by N. Oda and K. Takayanagi (North Holland Publishing Company, New York, 1980), pp. 125-143, and references therein; Y. Awaya, ibid., pp. 325-336, and references therein.
2. F. J. deHeer, J. Schutten, and H. Moustafa, Physica 32, 1766 (1966).
3. K. H. Berkner, W. G. Graham, R. V. Pyle, A. S. Schlachter, J. W. Stearns, and R. E. Olson, J. Phys. B 11, 875 (1978).
4. K. H. Berkner, W. G. Graham, R. V. Pyle, A. S. Schlachter, and J. W. Stearns, to be submitted to Physical Review A.
5. C. L. Cocke, Phys. Rev. A. 20, 749 (1979).
6. H. K. Haugen, P. Hvelplund, and H. Knudsen, in Electronic and Atomic Collisions, XIth International Conference in the Physics of Electronic and Atomic Collisions, edited by K. Takayanagi and N. Oda (Society for Atomic Collision Research, Japan 1979), pp. 588-589.
7. H. F. Beyer, K-H. Schartner, and F. Folkmann, J. Phys. B 13, 2459 (1980).

8. R. E. Olson and A. Salop, Phys. Rev. A 16, 531 (1977).

9. R. E. Olson, Phys. Rev. A 18, 2464 (1978).

10. R. E. Olson. J. Phys. B 12, 1843 (1979).

11. J. M. Hansteen and O. P. Mosebekk, Phys. Rev. Lett. 29, 1361 (1972).

12. J. H. McGuire and L. Weaver, Phys. Rev. A 16, 41 (1977).

13. R. E. Olson, K. H. Berkner, W. G. Graham, R. V. Pyle, A. S. Schlachter, and J. W. Stearns, Phys. Rev. Lett. 41, 163 (1978).

14. We previously briefly reported some of these measurements: K. H. Berkner, W. G. Graham, R. V. Pyle, A. S. Schlachter, and J. W. Stearns, Bull. Amer. Phys. Soc. 23, 1108 (1978); 24, 764 (1979).

15. C. F. Fischer, The Hartree-Fock Method for Atoms (Wiley, New York 1977), pp 28-34.

16. L. C. Northcliffe and R. F. Schilling, Nucl. Data Tables A 7, 233 (1970).

17. H. D. Hagstrum, Phys. Rev. 96, 325 (1954). The observed effect in our measurements with D^+ incident on dirty collector plates is only one fourth of that predicted using these secondary-electron-emission coefficients for clean surfaces.

18. B. A. Huber, J. Phys. B 13, 809 (1980).

19. H. Klinger, A. Muller, and E. Salzborn, J. Phys. B 8, 230 (1975).

20. C. Bottcher, J. Phys. B 10, L445 (1977).

21. N. Bohr and J. Lindhard, K. Dan Vidensk. Selsk., Mat.-Fys. Medd. 28, 1 (1954).

22. T. J. Gray, C. L. Cocke, and E. Justiniano, Phys. Rev. A. 22, 849 (1980).

TABLE I. Experimental net-ionization cross sections, σ_+, in units of 10^{-16} cm^2.

Projectile Ion	Energy (MeV/amu)	Target He	Ne	Ar	Xe
C^{+4}	1.14	3.2 + 0.4 - 0.5	8.6 + 1.0 - 1.3	20 + 2 - 3	
C^{+5}	0.31	10.0 + 1.1 - 1.5	20 + 2 - 3	56 + 7 - 9	
C^{+5}	1.14	4.4 + 0.5 - 0.7	11.3 + 1.3 - 1.7	26 + 3 - 4	
C^{+6}	0.31	13.0 + 1.6 - 2.1			
C^{+6}	1.14	6.15 + 0.7 - 0.9	15.3 + 1.7 - 2.3	35 + 4 - 5	
C^{+6}	4.75		8.0 + 0.9 - 1.2	20 + 3 - 4	44 + 7 - 9
Fe^{+12}	1.16			122 + 12 - 18	
Fe^{+18}	1.16			208 + 21 - 31	
Nb^{+23}	3.55			195 + 20 - 30	
Nb^{+31}	3.43			280 + 30 - 40	
Nb^{+34}	3.43			335 + 40 - 50	
Pb^{+54}	4.65			640 + 70 - 100	1560 + 190 - 250

Figure Captions

1. Schematic diagram of the apparatus. Net ionization cross sections were measured by collecting slow-ion and slow-electron current in the gas target.
2. Experimental net-ionization cross sections for 310 keV/amu C projectiles in charge states 5 and 6 in He(●), Ne (■), and Ar (▲) targets.
3. Net-ionization cross sections for 1.1 MeV/amu projectiles in charge state q in He (●,○), Ne (■,□), and Ar (▲,△) targets. The closed symbols are present experimental results (C and Fe projectiles), the open symbols are experimental results from Ref. 5 (Cl projectiles), and the lines are the CTMC calculations.
4. Net-ionization cross sections for 3.4 MeV/amu Nb projectiles in charge state q in an Ar target. The points are experimental results and the lines are the CTMC calculations.
5. Net-ionization cross sections for 4.8 MeV/amu C and 4.7 MeV/amu Pb projectiles in charge state q in Ne (■), Ar (▲), and Xe (▼) targets. The points are experimental results and the lines are the CTMC calculations for 4.7 MeV/amu.
6. Theoretical net-ionization cross sections: reduced plots of CTMC net-ionization cross sections for a highly stripped ion in charge-state q in He, Ne, Kr, Ar, and Xe targets. These calculations were performed for projectiles in the energy range 1-5 MeV/amu and with charge states q = +5 to +80.
7. Reduced plot of net-ionization cross sections for a highly stripped

ion in charge-state q in He (●) and Ar (▲) targets [Fig. 7(a)] and in Ne (■) and Xe (▼) targets [Fig. 7(b)]. The closed symbols are experimental results, and the curves are from the calculated points given in Fig. 6.

8. Calculated cross sections σ_j for production of Ar recoils j-times ionized, by incident 1-5 MeV/amu projectiles in charge states +80, +40, +20, +10, and +5.

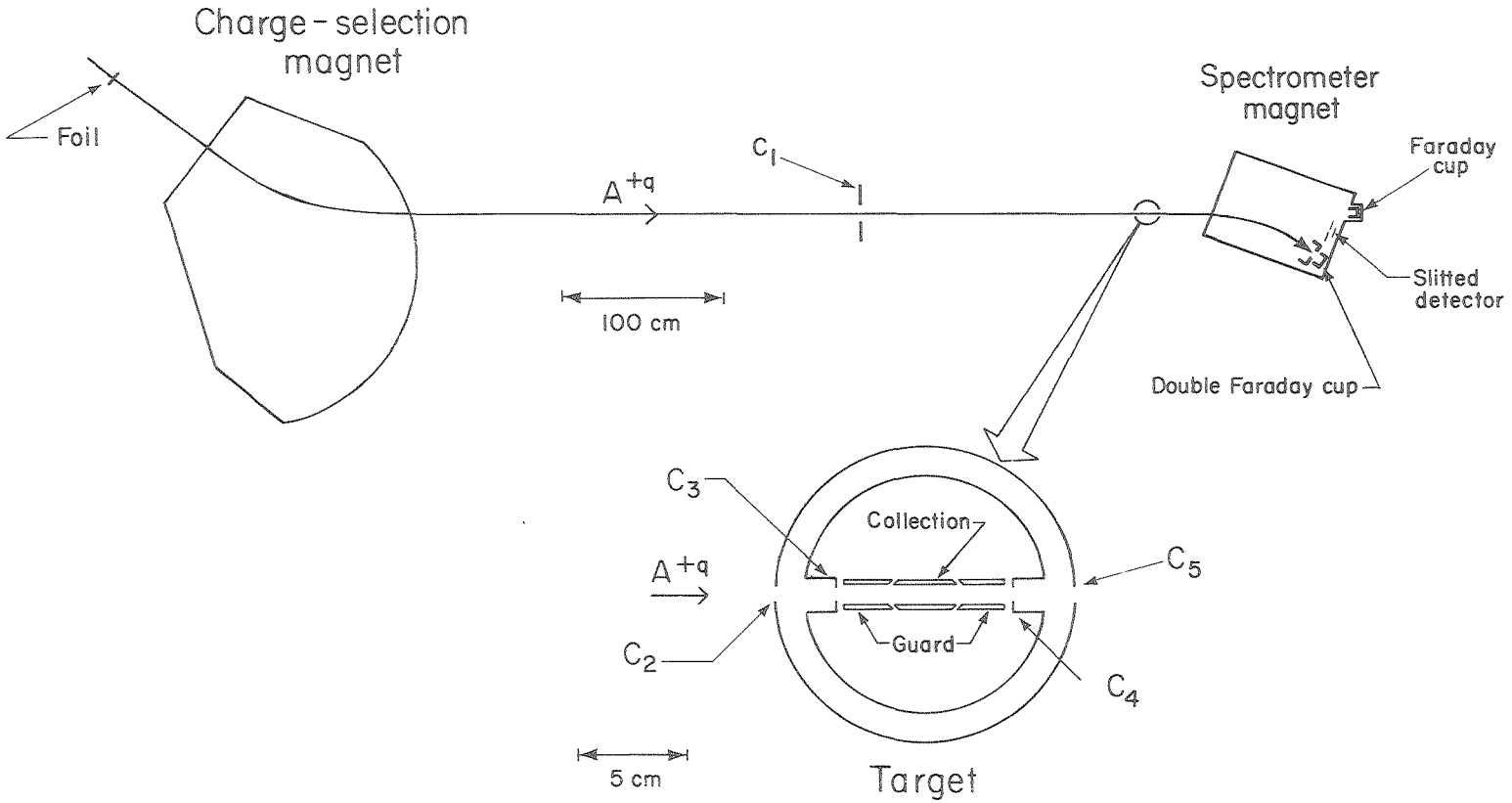
Charge - selection magnet
Foil
A^{+q}
C_1
100 cm
Spectrometer magnet
Faraday cup
Slitted detector
Double Faraday cup
C_3
Collection
A^{+q}
C_5
C_2
Guard
C_4
5 cm
Target
XBL 805-918A

Fig. 1

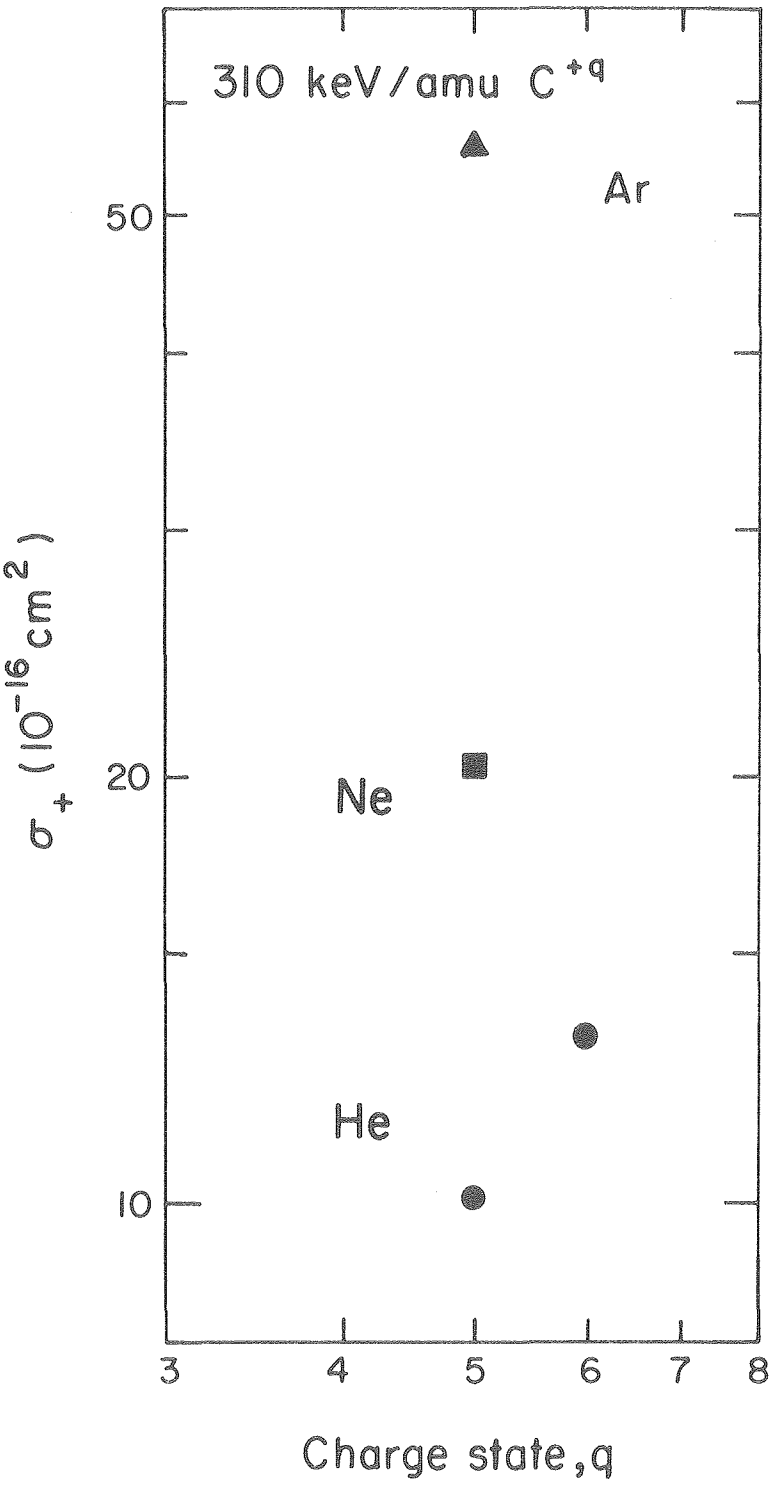

XBL807-1560

Fig. 2

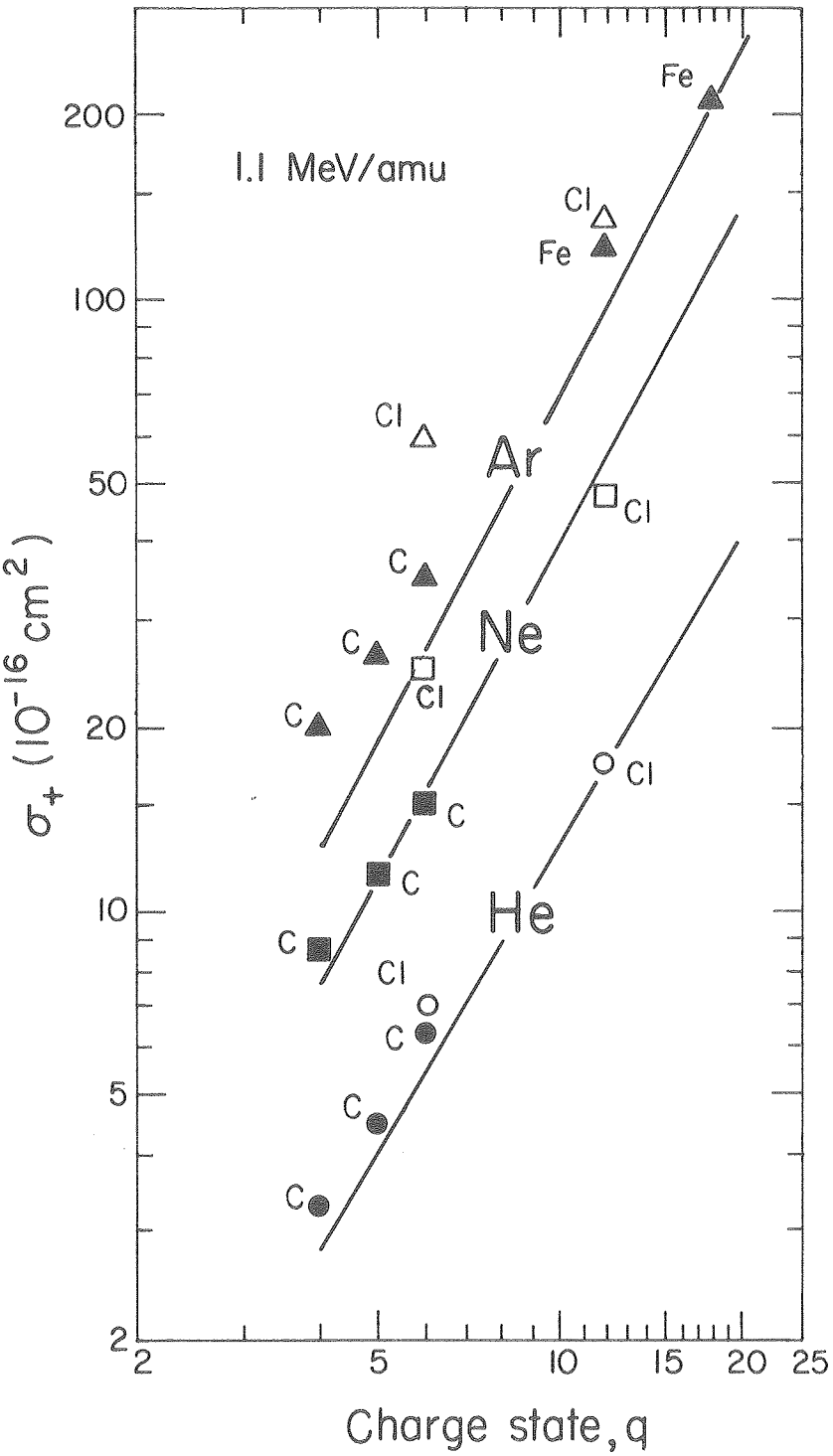

XBL 808-1564

Fig. 3

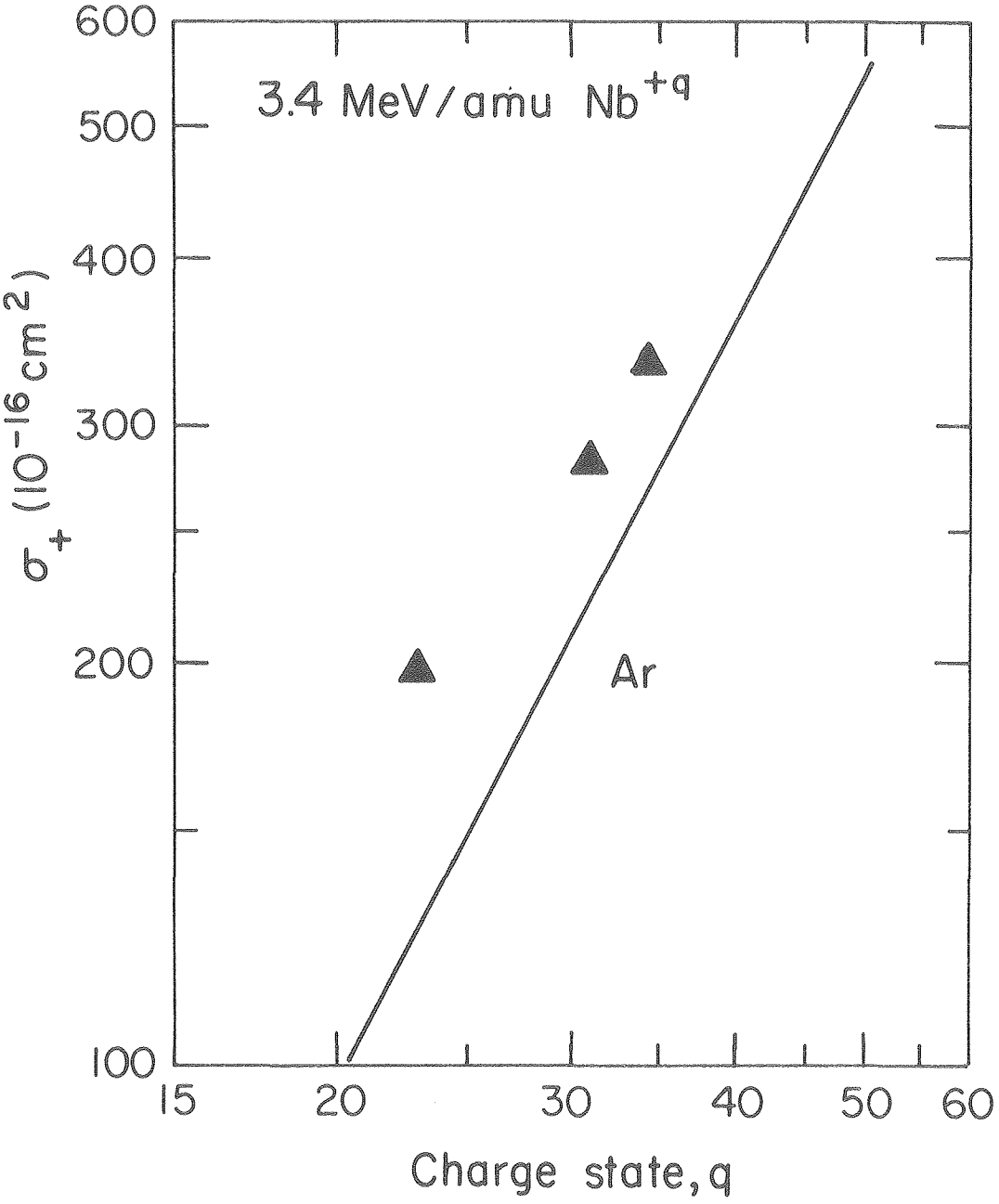

XBL 807-1562

Fig. 4

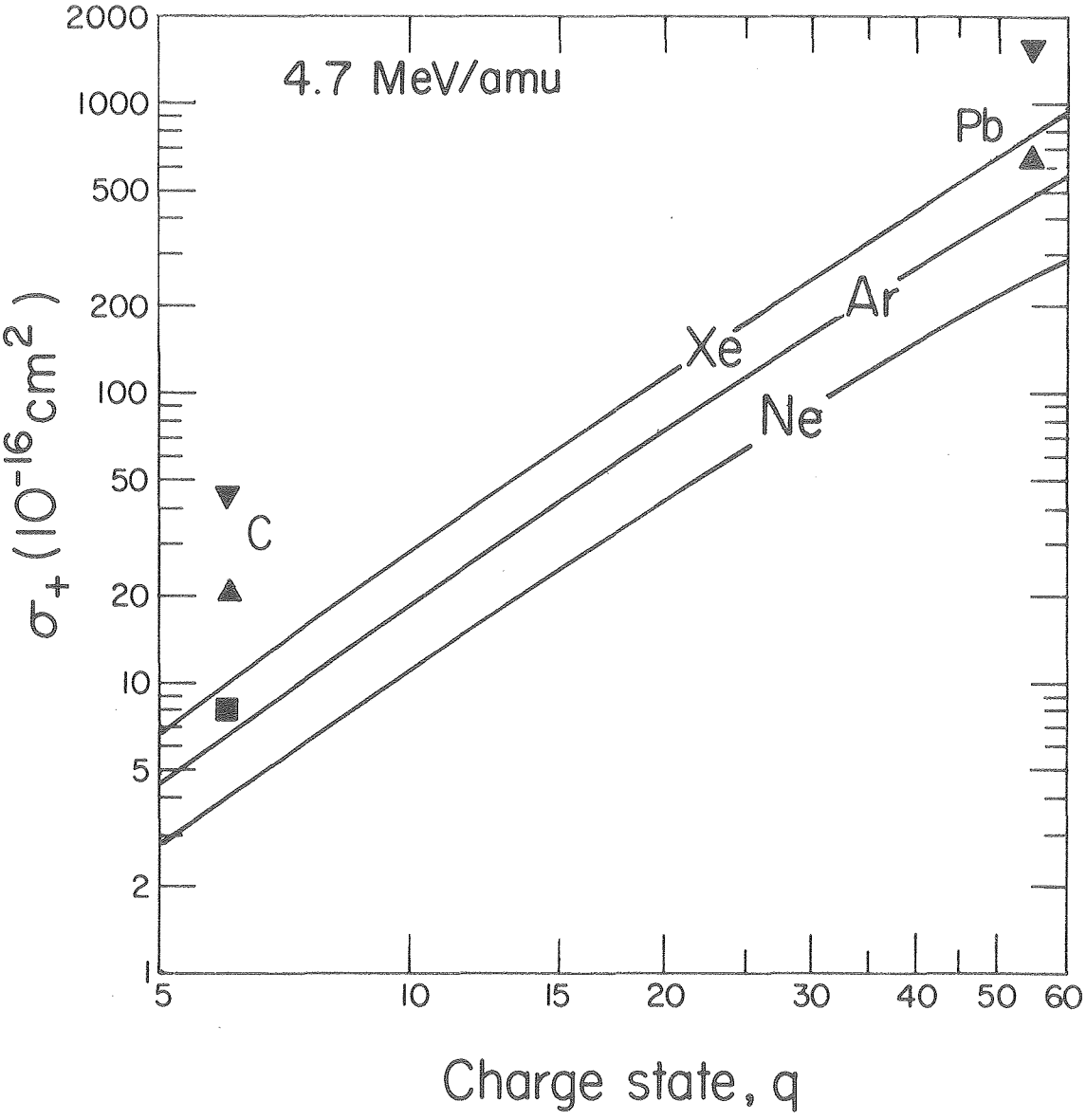
4.7 MeV/amu
Pb
Ar
Xe
Ne
C
σ_+ (10^{-16} cm^2)
2000
1000
500
200
100
50
20
10
5
2
1
5
10
15
20
30
40
50
60
Charge state, q
XBL 808-1563

Fig. 5

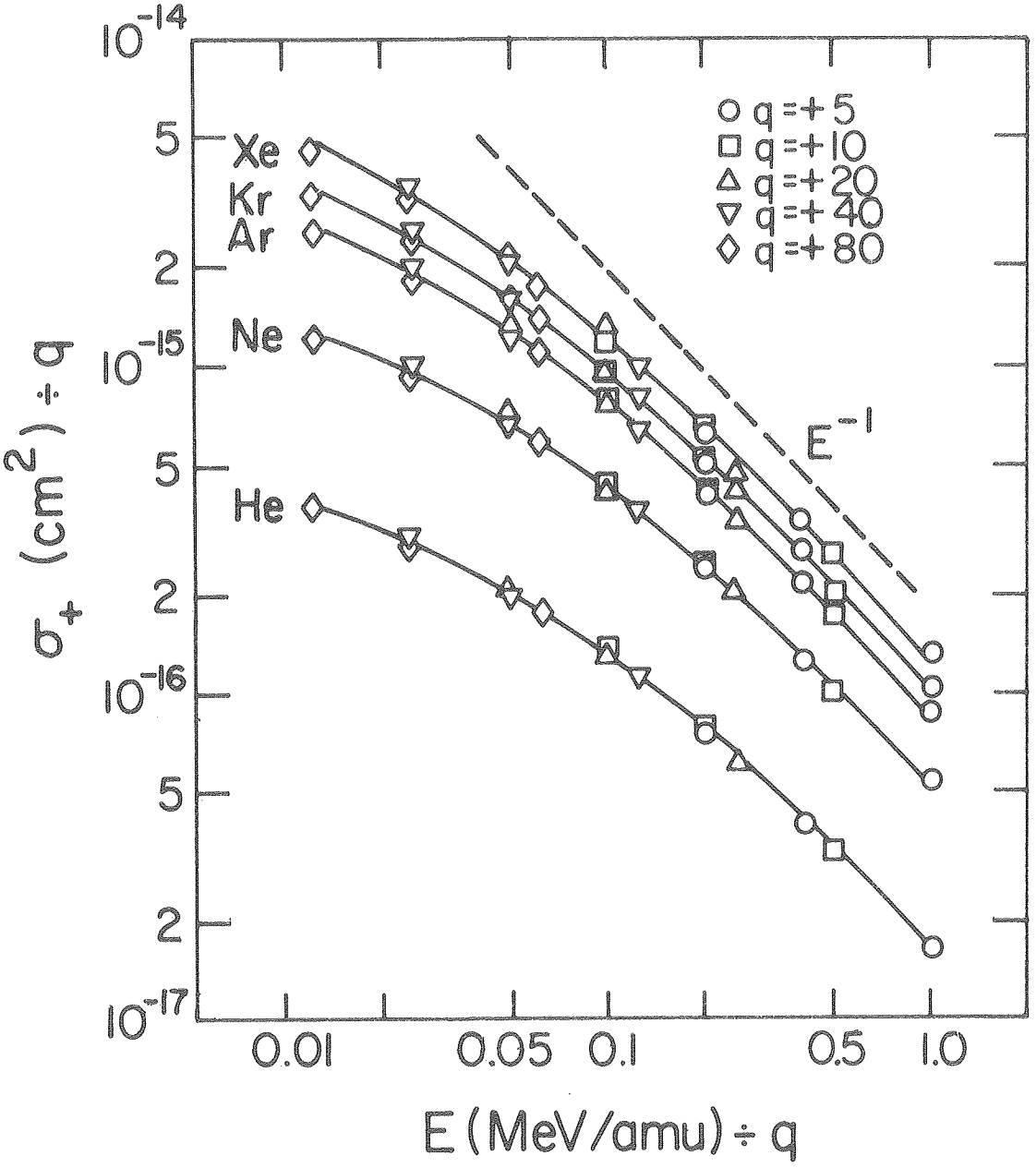

XBL808-1715A

Fig. 6

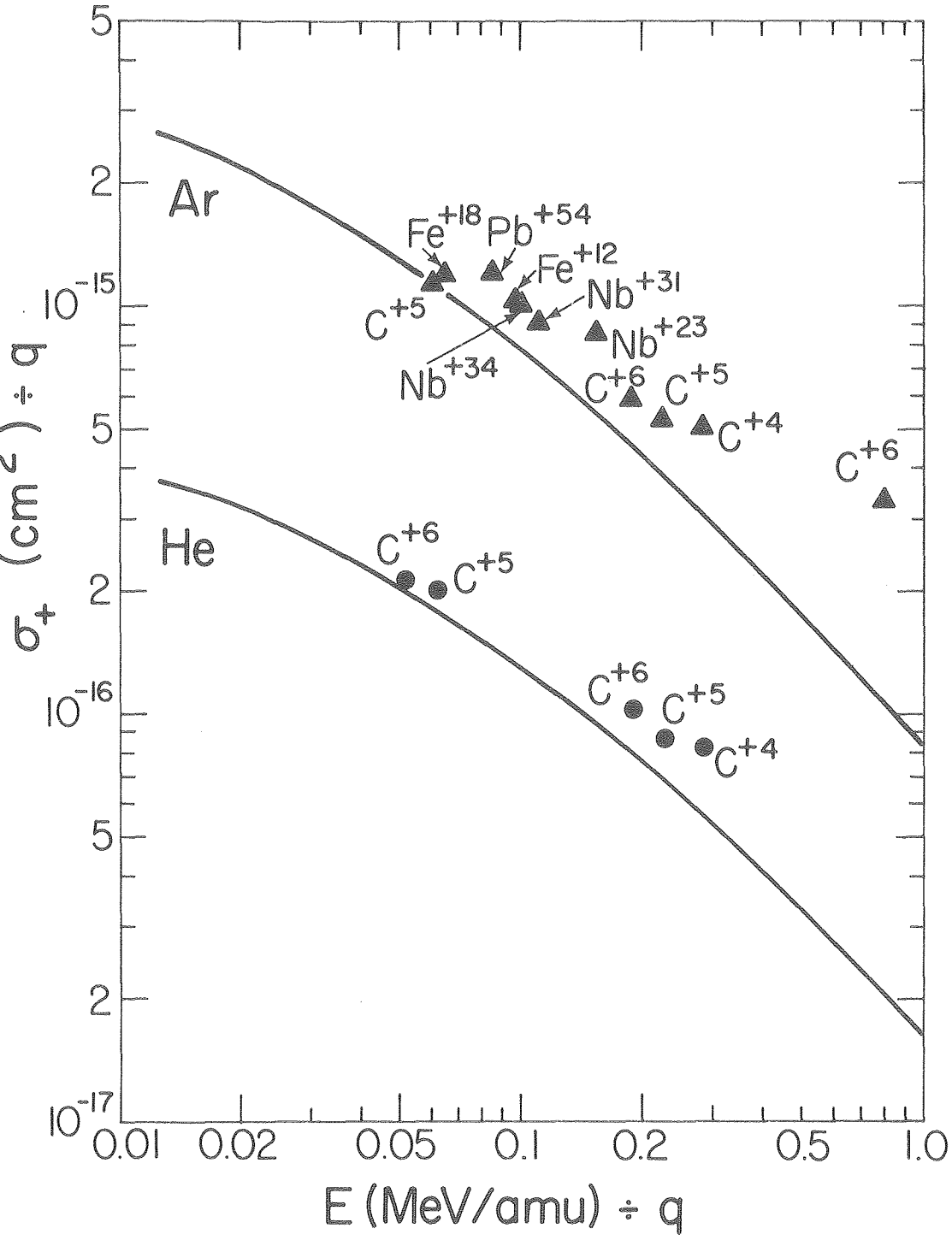

XBL 8010-2090

Fig. 7a

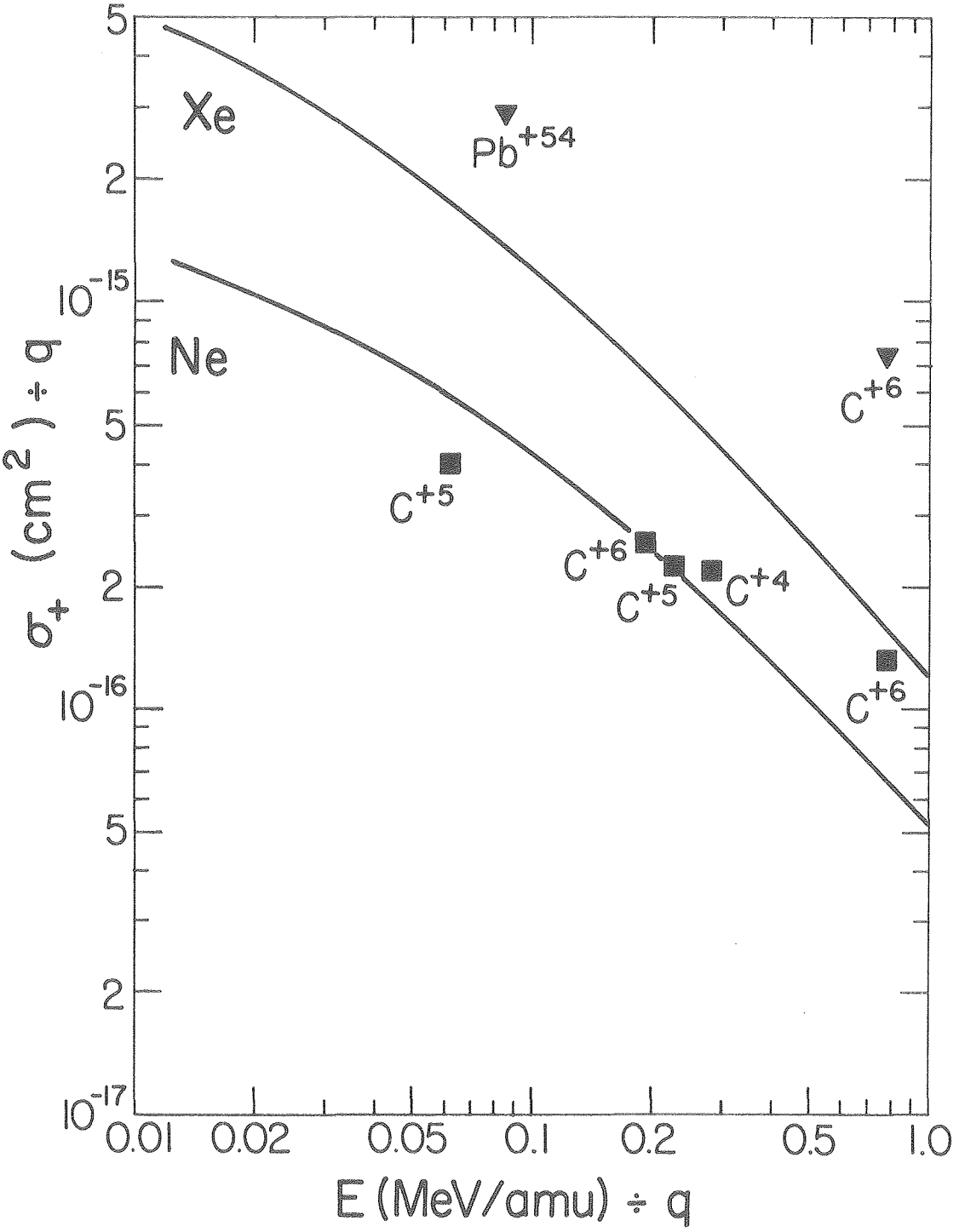

XBL 8010-2091

Fig. 7b

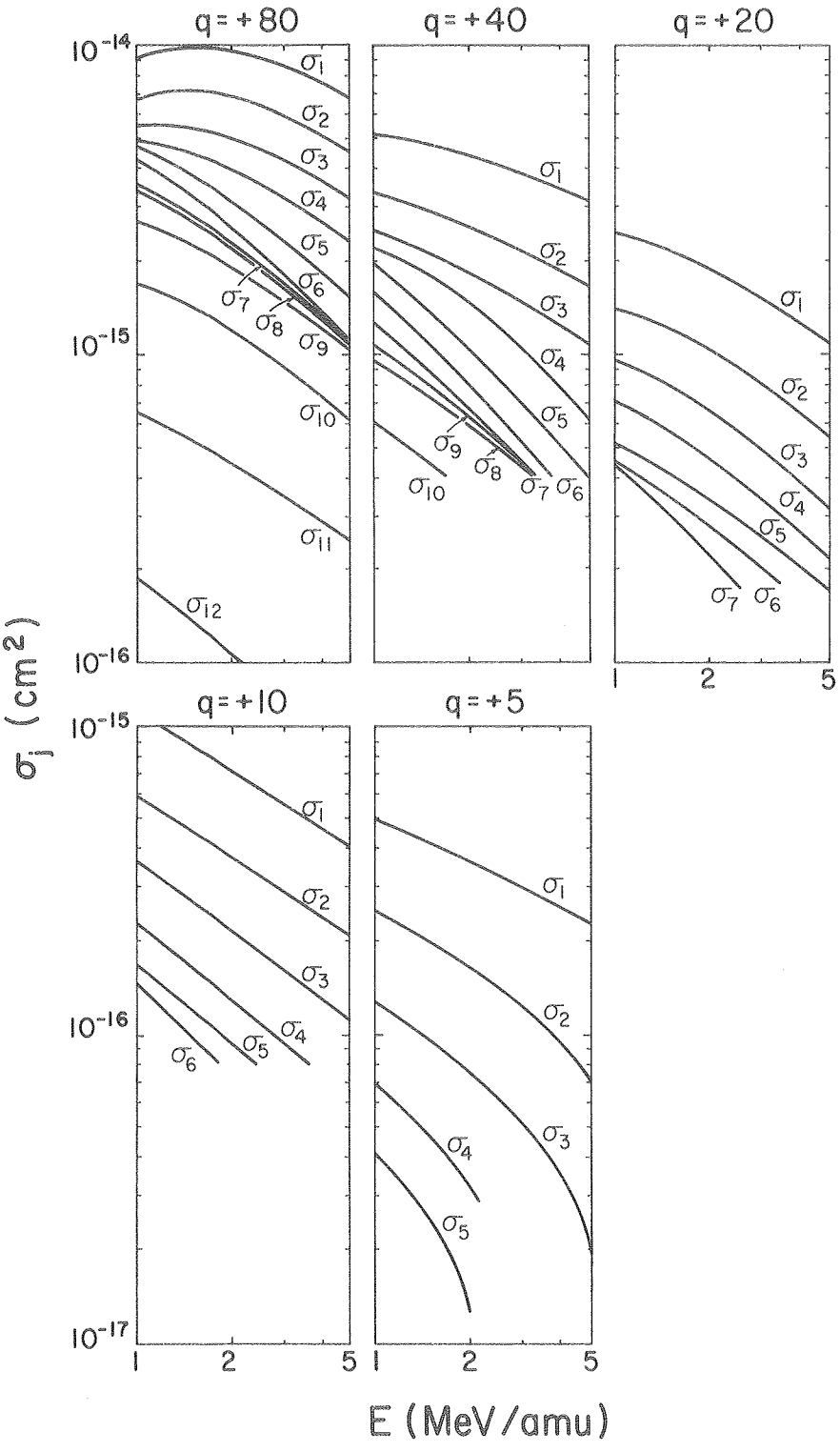

XBL 808-2735

Fig. 8